Research Article

Algae 2024, 39(3): 187-205
https://doi.org/10.4490/algae.2024.39.8.23
Open Access

Exploring the nutritional biochemical profiles and biological functions in the green microalga *Chlorella fusca*

Young Min Lee[1], Youn-Sig Kwak[2], Yong Bok Lee[3], Eun Young Seo[1] and Jin Hwan Lee[1,*]

[1]*Department of Life Resource Industry, Dong-A University, Busan 49315, Korea*
[2]*Department of Plant Medicine and RILS, Gyeongsang National University, Jinju 52828, Korea*
[3]*Institute of Agriculture & Life Science, Gyeongsang National University, Jinju 52828, Korea*

Chlorella species of microalgae are utilized in the crop and food industries. The aim of this research was to investigate the metabolite profiles of *Chlorella fusca* for the first time and evaluate its biological properties. The two ion modes of UPLC-Q-TOF-MS/MS were used to identify a total of 62 components in the methanol extract of *C. fusca*, with 26 in the negative and 36 in the positive ion mode, including 10 identical ingredients. Fatty acids (negative mode) and combinations of chlorophyll and fatty acids (positive mode) were the most prevalent chemical structures, constituting over 80 and 70% of the total metabolites, respectively, followed by chlorophyll, polar lipids, carotenoids, and fatty alcohols. Moreover, this extract exhibited potent antioxidant and anti-aging benefits in decreasing order of potency at a concentration of 200 μg mL^{-1}: tyrosinase inhibition (100%), ABTS radical scavenging (90%), elastase inhibition (88%), and DPPH radical scavenging (34%). Notably, this extract protected the mobility of DNA fragments up to 5 μg mL^{-1} (26%), with potential effects (> 60% at 200 μg mL^{-1}). These findings suggest that *C. fusca* may be a promising candidate for applications related to its biological functions, owing to the high accumulation of fatty acids and chlorophyll derivatives.

Keywords: biological function; *Chlorella fusca*; fatty acid; ion mode; metabolite; UPLC-Q-TOF-MS/MS

Abbreviations: ABTS, 2,2′-azino-bis(3-ethylbenzthiazoline-6-sulphonic acid); DPPH, 2,2-diphenyl-1-pycrylhydrazyl; DTT, dithiothreitol; GA, gallic acid; GAE, gallic acid equivalents; LPE, lysophosphatidylethanolamine; MCO, metal-catalyzed oxidation; PC, phosphatidylcholine; PG, phosphatidylglycerol; PI, phosphatidylinositol; QE, quercetin; TFC, total flavonoid content; TPC, total phenolic content; UPLC-Q-TOF-MS, ultra-high performance liquid chromatography coupled with quadrupole time-of-flight mass spectrometry

INTRODUCTION

Numerous studies have reported that microalgae (microscopic phytosynthetic organisms) living in both fresh water and sea water are widely used in the food, cosmetic, and pharmaceutical industries, as well as in various commercial applications (Kotrbáček et al. 2015, Safarfar et al. 2015, Habashy et al. 2018, El-fayoumy et al. 2021, Canelli et al. 2022, Ferdous et al. 2023). This source has attracted attention in the agricultural and biotechnological fields because of its utility in biofuel production and valuable chemicals (Musharraf et al. 2012, Gorgich et al. 2021, Zhou et al. 2022, Kang et al. 2023, Won et al. 2023). Specifically, microalgae are currently used to evaluate green biodiesel production under transesterification conditions (Mata et al. 2010, Musharraf et al. 2012, Kotrbáček et al. 2015, Zhou et al. 2022). Considering the observations stated above, these organisms have evolved from

Received April 12, 2024, **Accepted** August 23, 2024
***Corresponding Author**
E-mail: schem72@dau.ac.kr
Tel: +82-51-200-7521, Fax: +82-51-200-7505

food materials to being an energy feedstock and excellent source of chemical products in the modern age. Currently, microalgae are of increasing interest to the medicinal and functional food industries owing to their diverse benefits. Many researchers have demonstrated that microalgal metabolites are crucial for expanding food and nutraceutical applications (Kotrbáček et al. 2015, Yun et al. 2020, Gorgich et al. 2021, Canelli et al. 2022, Ferdous et al. 2023). Other studies have revealed the presence of various metabolites in microalgae, including polysaccharides, peptides, triterpenoids phenolics, fatty acids, proteins, amino acids, and chlorophyll derivatives (Montes D'Oca et al. 2011, López-Pacheco et al. 2019, Fernandes and Cordeiro 2020, Pantami et al. 2020, Kim et al. 2022, Kang et al. 2023). Furthermore, these constituents are associated with a wide range of human health benefits such as anti-inflammatory, antioxidant, antimicrobial, antitumor, and anti-allergic properties (Habashy et al. 2018, Vello et al. 2018, Gorgich et al. 2021, Kim et al. 2022, Ferdous et al. 2023, Kang et al. 2023, Zhou et al. 2023). It has recently been documented that microalgae have excellent characteristics, including fast growth, high photosynthetic rates in a short time, high protein content, high CO_2 capture ability, and the ability to convert solar energy to electrical energy (Vello et al. 2018, Deamici et al. 2019, Fernandes and Cordeiro 2020, Martini et al. 2021, Won et al. 2023). Among the various microalgae, the genus *Chlorella* is a single-celled organism of the Chlorophyta that is present in both fresh and marine water (Montes D'Oca et al. 2011, Sotoudehniakarani et al. 2019, Yun et al. 2020, Canelli et al. 2022, Chae et al. 2023). This material is used in fortified (or supplementary) foods, such as puffs, bread, pasta, juice, and cookies, to enhance their color and nutritional quality (Kotrbáček et al. 2015, Fernandes and Cordeiro 2020, El-fayoumy et al. 2021, Gorgich et al. 2021). In particular, *Chlorella* is a well-known rich source of metabolites, including dietary fiber, vitamins, carbohydrates, lipids, chlorophylls, and proteins, with a variety of health benefits (Ando et al. 2004, Kotrbáček et al. 2015, Pantami et al. 2020, Conde et al. 2021, Kim et al. 2022, Ferdous et al. 2023). Additionally, thousands of tons of *Chlorella* are produced annually in East Asia, Europe, and the United States and are now sold as nutraceutical or functional products (Mata et al. 2010, Musharraf et al. 2012, Safi et al. 2014, Safarfar et al. 2015, Sotoudehniakarani et al. 2019, Martini et al. 2021). It has been commonly established that *Chlorella* comprises several species, such as *C. vulgaris*, *C. pyrenoidosa*, *C. zofingiensis*, *C. ellipsoidea*, and *C. sorokiniana* (Montes D'Oca et al. 2011, Sotoudehniakarani et al. 2019, Yun et al. 2020, Gorgich et al. 2021, Martini et al. 2021, Chae et al. 2023), specifically, *C. vulgaris* and *C. sorokiniana* are agents of green healthy food approved by the Food and Agriculture Organization of the United Nations because of their nutrient profiles and widespread human consumption (Kotrbáček et al. 2015). It is well established that *C. fusca* and *C. vulgaris* are closely related green microalgae species (Bock et al. 2011, Deamici et al. 2019, Sotoudehniakarani et al. 2019). Although they share many similarities, such as their unicellular structure and autotrophic metabolism, they also exhibit distinct differences in terms of their cell size, growth characteristics, taxonomic positioning, and habit preferences (Bock et al. 2011, Deamici et al. 2019, Chae et al. 2023). In addition, *C. fusca* has been reported to have a lower food and commercial utilization potential than *C. vulgaris* (Mata et al. 2010, Safi et al. 2014, Kotrbáček et al. 2015). To date, several researchers have elucidated the distribution and composition of metabolites in *Chlorella* species, namely, *Chlorella* sp., *C. vulgaris*, *C. pyrenoidosa*, and *C. sorokiniana* (Montes D'Oca et al. 2011, Safi et al. 2014, Safarfar et al. 2015, Habashy et al. 2018, Fernandes and Cordeiro 2020, Pantami et al. 2020, Canelli et al. 2022, Montoya-Arroyo et al. 2022), however, to the best of our knowledge, there is no comprehensive information available on the characterization of the metabolite profile of *C. fusca*. Moreover, there are few published studies on the simultaneous determination of individual components to obtain chemical profiles using the ultra-high performance liquid chromatography-quadruple-time of flight-mass spectrometry (UPLC-Q-TOF-MS/MS) method in both negative and positive ion modes. Little information is available on the comparison and demonstration of the biological functions of *C. fusca* extract. Therefore, our study was designed to obtain information regarding metabolite constituents, as well as their as antioxidant and anti-aging abilities, using the two ion modes of TOF-MS.

The key objective of the current work was to identify the metabolite profiles in the methanol extract of *C. fusca*. We investigated herein, for the first time, the comparison and characterization of metabolite profiles with the application of negative and positive ion modes using the UPLC-Q-TOF-MS/MS technique to screen as many potential metabolites as possible for an in-depth analysis of this resource. In addition, this study documented the antioxidant activities of radical scavenging and DNA protection, as well as the total phenolic and total flavonoid contents of antioxidative substances. Our research is also the first to assess the inhibitory capacities of anti-aging factors against tyrosinase and elastase.

MATERIALS AND METHODS

Microalgae source and reagents

The freshwater microalgae *C. fusca*, was used in the present study. The CHK0059 strain of *C. fusca* was provided by the National Institute of Agricultural Science of the Rural Development Administration, Wanju, Jeonbuk Province, Republic of Korea. The microalgae were cultivated at F&B Nature Co. Ltd. (Chungju, Korea) as follows: initial inoculation, 1×10^6 cells mL^{-1}; temperature, 28°C; period, 6 d; light, 120 μm m^{-2} s for 24 h in a day; air circulation, 2 L min^{-1}. Cultured microalgae were collected on Mar 10, 2021, and their appearance is shown in the Supplementary Fig. S1. This material was immediately stored at 0°C prior to analysis. The pUC19 super-coiled plasmid DNA was supplied by Thermo Fisher Scientific (Waltham, MA, USA). 2,2-diphenyl-1-picrylhydrazyl (DPPH), 2,2′-azinobis(3-ethylbenzthiazoline-6-sulphonic acid) (ABTS), tyrosinase (EC 1.14.18.1), elastase (EC 3.4.21.36), ascorbic acid, 6-hydroxy-2,5,7,8-tetramethylchroman-2-carboxylic acid (Trolox), ursolic acid, $FeCl_3$, dithiothreitol (DTT), L-tyrosine, *p*-nitrophenyl-α-D-glucopyranoside, *p*-nitrophenol, *p*-nitrophenol-β-D-glucopyranoside, gallic acid (GA), and quercetin (QE) were obtained from Sigma-Aldrich (St. Louis, MO, USA). The total phenolic content (TPC; Folin-Ciocalteu reagent and sodium carbonate) and total flavonoid content (TFC; sodium nitrite, sodium hydroxide, and diethylene glycol) were also provided by Sigma-Aldrich. Other chemicals and solvents, such as UPLC-MS grade water and acetonitrile (J.K. Baker, Phillipsburg, NJ, USA), were used at analytical grade without further purification.

Equipment

To measure the biological properties of the antioxidant, tyrosinase, and elastase, UV-Vis absorption spectra were used on an Agilent BioTeck microplate spectrophotometer (EPOCH2; BioTek Instruments, Winooski, VT, USA). The TPC and TFC analyses were also performed using this spectrometer. Multiple metabolite compositions were confirmed by a UPLC system (UPLC SCL40 Nexera X3 series; Shimadzu, Kyoto, Japan) coupled with a triple quadruple time-of-flight tandem mass spectrometry (LC/MS-Triple TOF X500R; AB SCIEX, Framingham, MA, USA) equipped with an electrospray ionization interface. Data acquisition and processing were performed by a preliminary TOF-MS high-resolution full scan, following the SWATH protocol (AB SCIEX, Foster City, CA, USA).

Preparation of *Chlorella fusca* extract

For metabolite analyses and biological assays, the cultured *C. fusca* samples were separated from the solution and supernatant by centrifugation (3,000 ×g, SL 40R; Thermo Fisher Scientific). The collected supernatant was air dried at 25°C for 2 d to remove the moisture, and then the dried green powder (1 g) was extracted with 20 mL of methanol in a shaking incubator for 3 d at 25°C. Extraction was performed with slight modifications to previously reported methods (Habashy et al. 2018, Vello et al. 2018). The crude methanol extract was centrifuged at 3,000 ×g for 5 min and filtered through Whatman filter paper (No. 42; Sigma-Aldrich). The filtered solution was examined for antioxidant and anti-aging properties as well as TPC and TFC. Also, this solution was filtered through a syringe filter (0.45 μm; Whatman Inc., Maidstone, UK) prior to UPLC-TOF-MS analysis.

Analyses of TPC and TFC

The material for TPC and TFC (mg g^{-1}) were prepared as described in subsection 2.3 (1 g of dried sample in 20 mL methanol). The TPC analysis was performed using the Folin-Ciocalteu reagent with slight modifications (Safarfar et al. 2015, Ha et al. 2021), and TFC was measured by the colorimetric method as described by Safarfar et al. (2015) and Ha et al. (2021). In brief, the methanol extract (500 μL) of *C. fusca* was mixed with 2 N Folin-Ciocalteu's reagent (250 μL) and distilled water (250 μL), and then incubated for 1 h at 25°C. Sodium carbonate solution (20%, 500 μL) was added to the Ciocalteu reaction mixture and incubated for 10 min at 35°C. The absorbance value was measured at 750 nm by a spectrophotometer and compared to a calibration curve (GA, 0.5–500 μg mL^{-1}). The content was expressed as milligrams of gallic acid equivalents (GAE) per g of dried sample. The TFC method was also carried out according to previous research using the colorimetric technique (Safarfar et al. 2015, Ha et al. 2021). The sample extract (250 μL) was added to methanol (2 mL) followed by 90% diethylene glycol (1 mL) and 4 M NaOH (1 mL). After heating at 35°C for 10 min, the absorbance of the reaction mixture was determined using a spectrophotometer at 420 nm and compared with the calibration curve (QE, 0.5–500 mg mL^{-1}). This result was calculated as mg of QE per g of dried sample. The TPC and TFC ratios were determined in three independent experiments (mean values) for each triplicate sample.

Antioxidant abilities against radical sources

The antioxidant properties of DPPH and ABTS radicals in the methanol extract of *C. fusca* (1 g, 20 mL) were determined as described by Ha et al. (2021) and Lee et al. (2023). A sample or positive control (ascorbic acid) (0.1 mL) of six different concentrations (25–600 μg mL^{-1}) was mixed with methanol (0.49 mL), and then added to a 1 mM DPPH methanolic solution (0.39 mL). The crude solution was vortexed at 25°C for 30 min in the dark, and the absorbance of the reaction mixture was measured at 517 nm. The DPPH radical scavenging effect was evaluated as a percentage by the following equation:

Scavenging activity (%) = [(1 - sample absorbance value/control absorbance value)] × 100

The ABTS radical scavenging properties were determined on the capacities of different substances to the radical cation scavenge by comparison with the positive control (Trolox) using a spectrophotometer at 734 nm. This radical cation source of 7 mM ethanolic solution was generated by reacting the $ABTS^{\bullet+}$ stock solution with potassium persulfate ($K_2S_2O_8$, 2.45 mM), and allowing to stand at 25°C for 12 h in darkness. The crude solution was diluted in EtOH (abs 0.70). A sample extract or positive control (0.1 mL) of four concentrations (25–200 μg mL^{-1}) was added to 0.9 mL of $ABTS^{\bullet+}$ solution. After vortexing for 1 min at 25°C, the absorbance value was measured using a spectrophotometer. This capacity was calculated as a percentage according to the following formula:

Scavenging activity (%) = [(control absorbance value - sample absorbance value)/control absorbance value] × 100

Antioxidant capacities were based on three replicate samples with mean values.

DNA protective effect

A metal-catalyzed oxidation (MCO) DNA cleavage protection assay was conducted as described by Lee et al. (2023). In brief, the methanol extracts of *C. fusca* at different concentrations were added to 3.3 mM DTT (5 μL) and 15.4 μM $FeCl_3$ (5 μL), and then incubated at 37°C for 2 h. The above reaction solution was mixed with pUC18 super-coiled plasma DNA (1 μg). After incubation for 2 h at 37°C, the mixture solution (5 μL) was added to DNA loading buffer (1 μL), and then loaded onto a 0.8% agarose gel in TAE buffer (1 mM EDTA and 40 mM Tris-acetate). After being electrophoresed (30 min at 85 V), the DNA in the gel was visualized and photographed using the Gel Doc XR+ system (Universal Hood II; Bio-Rad Laboratories, Hercules, CA, USA) equipped with a UV transilluminator and a camera. DNA band intensity and imaging were performed using Image Lab software (Bio-Rad Laboratories). The inhibition rate (%) of DNA damage (mean value of three independent experiments) was calculated by the following equation (Rahman et al. 2018, Seal et al. 2020):

DNA protection rate (%) = (SF DNA band intensity/pUC18 plasmid DNA band intensity) × 100

Enzyme inhibition effects

The inhibitory abilities against tyrosinase and elastase were measured in earlier studies, with slight modifications (Azmi et al. 2014, Lee et al. 2023), as the mean values of three independent experiments performed in triplicate. To prepare the tyrosinase inhibition assay, the diluted sample (30 μL) or ascorbic acid (positive control, 30 μL) was mixed in methanol with sodium phosphate buffer (NaH_2PO_4, 0.05 mM, pH 6.8, 970 μL). L-tyrosine solution (1,000 μL) was added and vortexed with tyrosinase (200 units mL^{-1}, 1,000 μL) for 1 min. The reaction solution was placed at 37°C for 30 min, and then monitored by spectrophotometry at a wavelength of 490 nm.

The inhibition rate was expressed as a percentage according to the following formula:

Inhibitory activity (%) = (control absorbance value - sample absorbance value/control absorbance value) × 100

Elastase inhibition ability was also demonstrated using a spectrophotometric method. The sample was dissolved in methanol at 1,000 μg mL^{-1}, and then diluted to various concentrations with 0.2 mM Tris-HCl buffer (pH 8.0). Elastase was dissolved to make a 3.33 mg mL^{-1} stock solution in Tris-HCl buffer (0.2 mM, pH 8.0) and the substrate *N*-succinyl-Ala-Ala-Ala-*P*-nitroanilide (1.6 mM) was diluted with the above buffer. The reaction solution contained Tris-HCl buffer (100 μL), substrate (25 μL), elastase (25 μL), and sample (50 μL) or ursolic acid (positive control, 50 μL) in a 96-well plate, and was incubated for 20 min at room temperature. Absorbance value of the crude solution was recorded at a wavelength of 410 nm. This enzyme inhibition rate was calculated as a percentage using the following equation:

Inhibitory activity (%) = (1 - absorbance value of sample extract/absorbance value of buffer) × 100

Conditions of UPLC-Q-TOF-MS/MS analysis for metabolite identification

The UPLC separation was performed on a Poroshell 120 Bonus-Rp (100 mm × 2.1 mm, 2.7 m; Agilent Technologies, Santa Clara, CA, USA). The mobile phase consisted of two solvents: (A) acetonitrile and (B) water containing 0.1% acetic acid. The metabolites were separated using the following gradient elution profile: 50% A in 0–5 min; 70% A in 5–15 min; 80% A in 15–25 min; 90% A in 25–30 min; 95% A in 30–40 min; 98% A in 40–45 min. The flow rate was 0.3 mL min^{-1} with an injection volume of 2 μL and the column temperature was carried out at 25°C. After chromatographic separation, the mobile phase was introduced directly into the Triple TOF X500R instrument. The MS system was operated in both negative and positive ion modes, with the mass range set at *m/z* 100–1,000 *Da* at full scan resolution. The operating MS conditions were as follows: (common conditions) ion source, turbolonspray; source temperature, 450°C; curtain gas, 30 psi; ion source gas 1: 50 psi and gas 2: 50 psi; accumulation time, 0.25 s. Nitrogen and argon were used as cone (40 L h^{-1}) and collision (600 L h^{-1}) gases; (other conditions of negative ion mode) ion spray voltage, -4,500 V; declustering potential, -80 V; collision energy, -10 V; declustering potential spred, 0 (other conditions of positive ion mode) ion spray voltage, 5,500 V; declustering potential, 50 V; declustering potential spread, 0; collision energy, 10 V; collision energy spread, 0. The raw data was controlled and acquired by Analyst TF1.7 software (AB SCIEX) with information-dependent acquisition packing. Metabolites were identified by comparison with their retention times, accurate mass, and MS/MS fragments in previous research on *Chlorella* species as well as elemental analysis (SCIEX OS software version 2.0; AB SCIEX, Foster City, CA, USA) and natural products databases (Massbank, Chemspider, and phytochemical dictionary).

Statistical analysis

All measurements, including TPC, TFC, antioxidant, and enzyme inhibition were expressed as the mean values of three replicates using Sigma Plot 2000 (SPSS Inc., Chicago, IL, USA).

RESULTS AND DISCUSSION

Evaluations of TPC and TFC in *Chlorella fusca* extract

The total amounts of phenolics and flavonoids were evaluated in the methanol extract of *C. fusca* by UV-Vis spectrophotometer. Their contents were assessed using linear standard curves of GA (TPC) and QE (TFC). In the current work, the TPC value was found to be 0.84 GAE mg g^{-1}, and the TFC was 1.89 QE mg g^{-1}. Our results differed significantly from prior observations, which stated that TPC and TFC in *C. vulgaris* were observed with 5.18 GA mg g^{-1} and 3.46 rutin (Ru) mg g^{-1} (Habashy et al. 2018). In general, these two factors displayed considerable differences depending on the extraction solvents (Ferdous et al. 2023). Furthermore, compared to earlier studies (MeOH extract: TPC, 13.32 GAE mg g^{-1}; TFC, 40.35 QE mg g^{-1}) (Ferdous et al. 2023), our data showed lower TPC and TFC ratios. Based on the above considerations, we confirmed that the presence of phenolic metabolites in the *C. fusca* extract was significantly lower than that in other *Chlorella* species. This phenomenon may be due to diverse environmental conditions affecting *Chlorella* growth, including growth patterns, genetics, and species, as shown in previous studies (Bock et al. 2011, Habashy et al. 2018, Deamici et al. 2019, Yun et al. 2020, Montoya-Arroyo et al. 2022). However, these two factors may not be key sources or contributors for determining the quality of *C. fusca*. Our research also demonstrated that phenolic metabolites were not the main components observed in this species using UPLC-Q-TOF-MS/MS analysis.

Measurement of antioxidant properties against DPPH and ABTS radicals in *Chlorella fusca* extract

For a comprehensive evaluation of the antioxidant properties in *C. fusca*, the present study demonstrated, for the first time, the scavenging activities on DPPH and ABTS radicals related to simple quality control and strong reproducibility (Safarfar et al. 2015, Rahman et al. 2018, Seal et al. 2020, EI-fayoumy et al. 2021, Ha et al. 2021). The antioxidant capacities at various concentrations compared to those of positive control (ascorbic acid) are shown in Fig. 1. Although extracts of *Chlorella* species have been studied for various functional factors such as antibacterial, anticancer, and antimicrobial activities (Safarfar et al. 2015, Habashy et al. 2018, EI-fayoumy et al. 2021, Gorgich et al. 2021, Ferdous et al. 2023, Zhou et al. 2023), there are no comprehensive reports on the an-

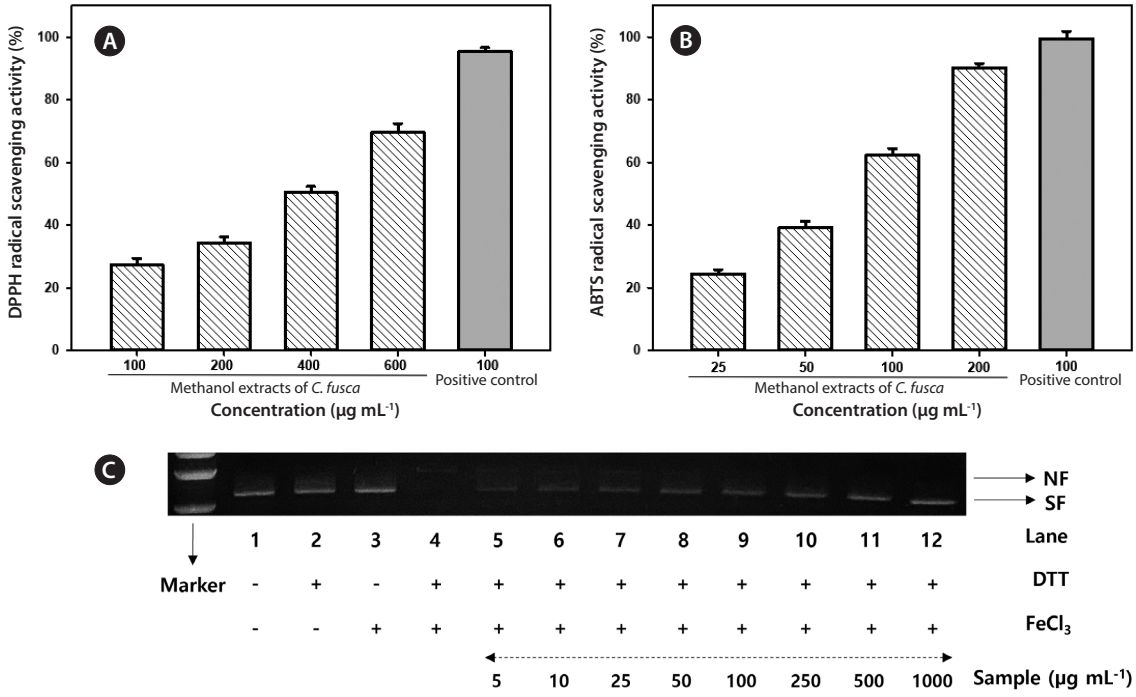

Fig. 1. Comparisons of antioxidant and DNA protectant properties in the methanol extract of *Chlorella fusca*. (A) DPPH (2,2-diphenyl-1-pycryl-hydrazyl) radical scavenging activities. (B) ABTS (2,2′-azino-bis(3-ethylbenzthiazoline-6-sulphonic acid)) radical scavenging activities. (C) DNA protectant activities. Lane 1, pUC18 only; lane 2, pUC18 with dithiothreitol (DTT) only; lane 3, pUC18 with $FeCl_3$ only; lane 4, pUC18 with metal-catalyzed oxidation (MCO) system; lanes 5–9, pUC18 with combinant extracts in the MCO system (lane 5: 5, lane 6: 10, lane 7: 25, lane 8: 50, lane 9: 100, lane 10: 250, lane 11: 500, and lane 12: 1,000 μg mL^{-1}). Nicked form (NF) and super-coiled form (SF) of the plasmid DNA are indicated by arrows.

tioxidant properties in *C. fusca* and little information is available on the radical scavenging effects of *Chlorella* extracts. For these reasons, we studied the dose-dependent antioxidant activities of methanol extracts of *C. fusca* and investigated their capacities by comparing the percentage inhibition patterns under the formation of DPPH and ABTS radicals. The DPPH radical scavenging capacities of the methanol extracts varied remarkably with concentrations. The scavenging activities of the individual samples and the positive control (ascorbic acid) increased with increasing concentrations (600, 400, 200, and 100 μg mL^{-1}) (Fig. 1A). The effects of the *Chlorella* extracts at different concentrations occurred in the following order: 70% at 600 μg mL^{-1}, 50% at 400 μg mL^{-1}, 34% at 200 μg mL^{-1}, and 27% at 100 μg mL^{-1}. This phenomenon suggests that the antioxidant capacities of *C. fusca* may be more affected by multiple metabolite constituents and contents, including tocopherols, carotenoids, fatty acids, and phenolics, compared to the results obtained with *C. vulgaris* in previous studies (Safarfar et al. 2015, Canelli et al. 2022, Kim et al. 2022, Ferdous et al. 2023, Zhou et al. 2023). Furthermore, *Chlorella* radical scavenging rates may be responsible for diverse factors, such as species, growth conditions, and genetics (Habashy et al. 2018, Yun et al. 2020, Gorgich et al. 2021). Another radical source, the scavenging abilities of ABTS radical also exhibited considerable differences in the individual concentrations (Fig. 1B), similar to the data obtained in the DPPH assay (Fig. 1A). The most potent ABTS radical scavenging ability was found in the *Chlorella* extract at 200 μg mL^{-1} (90%), and the remaining effects showed significant differences at each concentration as follows: 62% at 100 μg mL^{-1}, 39% at 50 μg mL^{-1}, and 24% at 25 μg mL^{-1} (Fig. 1B). In other words, their capacities increased with dose-dependent activation according to the increases of sample concentrations in the following rank order: 200 > 100 > 50 > 25 μg mL^{-1}, similar to those of the DPPH radical. Overall, all *Chlorella* extracts had higher radical scavenging abilities, approximately four-fold higher than that of the DPPH radical (Fig. 1A & B). These differences may be positively correlated with the reaction ratios between the radical sources and metabolites in the *Chlorella* extract, as observed in previous research crop studies (Rahman et al. 2018, Seal et al. 2020, Lee et al. 2023). Our results confirm that ABTS radical inhibition can be determined by the chain breaking and hydrogen donating effects of many metabolites (tocopherols,

carotenoids, fatty acids, etc.) in the methanol extract by comparison with the hydrogen donating characteristics of the DPPH radical reaction (Safarfar et al. 2015, Canelli et al. 2022, Lee et al. 2023). Moreover, the present data are consistent with earlier results on the antioxidant patterns of other *Chlorella* species (Canelli et al. 2022, Ferdous et al. 2023). Even though the methanol extract of *C. fusca* showed slightly lower abilities compared with the positive controls (DPPH: ascorbic acid; 70%, ABTS: Trolox; 92%, 200 μg mL^{-1}), the above findings reveal that *C. fusca* may serve as an active free radical scavenger and an excellent source of natural antioxidants. We believe that this material may provide several options for the development and utilization of functional agents for improving human health.

Measurement of DNA protection in *Chlorella fusca* extract

On the basis of the DPPH and ABTS radical scavenging capacities, to get more meaningful results on the antioxidant effect, we examined the super-coiled DNA protection rates of recombinants in the methanol extract of *C. fusca*. Briefly, the ability of this source to prevent hydroxyl radical-induced oxidative DNA damage was investigated at different concentrations based on the gel mobility in a MCO system. This assay was prepared by comparing the percentage protections using eight different concentrations (1,000, 500, 250, 100, 50, 25, 10, and 5 μg mL^{-1}) of the methanol extract (Fig. 1C). The defense patterns of DNA oxidation showed remarkable differences in the concentrations of the samples. As indicated in Fig. 1C, the methanol extracts were detected with low DNA damage protection (< 45%) at 50, 25, 10, and 5 μg mL^{-1} in comparison to those of the protection bands at high concentrations of 1,000, 500, 250, and 100 μg mL^{-1}. In detail, the DNA bands were protected with 86, 73, 63, and 51% after incubating the *C. fusca* extracts at 1,000, 500, 250, and 100 μg mL^{-1}, respectively, compared to that of the control (1 kb DNA marker pUC18 only) (Fig. 1C). Therefore, the antioxidant patterns showed high DNA protection rates (> 50% at 100 μg mL^{-1}) with markedly increasing activities according to the increases in sample concentrations. Although the potential DNA protection rates exhibited similar patterns as the data obtained from the radical scavenging assays, their activities were in the following order: ABTS > DNA protection > DPPH (ex. 62%; ABTS, 51%; DNA protection, 27%; DPPH at 100 μg mL^{-1}). These findings may be significantly influenced by the metabolite profiles and their contents, as well as the reaction portions, through antioxidant methods, as previously described (Rahman et al. 2018, Seal et al. 2020, Ferdous et al. 2023, Kang et al. 2023). From the current results, the methanol extract of *C. fusca* may be an excellent source for oxidative DNA damage protection in the nicked DNA through the MCO system. Our data provide valuable evidence that this source is beneficial human health. To the best of our knowledge, this is the first study to reveal that *C. fusca* extract has potential antioxidant properties related to radical scavenging and DNA cleavage factors.

Measurement of enzymatic inhibitions on tyrosinase and elastase in *Chlorella fusca* extract

To explore more available information, we measured enzyme inhibitory effects of *C. fusca* extract against tyrosinase and elastase. These enzymes have been the most prominant targets in the cosmetic industry owing to their skin whitening and anti-wrinkle properties (Ando et al. 2004, Azmi et al. 2014, Lee et al. 2023). Unfortunately, up to now, several literatures have not shown the relationship between the inhibition of these enzymes in *Chlorella* species. Therefore, we conducted the tyrosinase and elastase inhibitory capacities according to the percentage rates at each concentration of the *C. fusca* extract. Based on the antioxidant results and the previous experiments, the appropriate tyrosinase inhibition was achieved with high activity (93%) at 140 μg mL^{-1}. As illustrated in Fig. 2A, tyrosinase inhibition effects were observed with significant dose-dependent variations at different methanol extract concentrations. Specifically, the inhibitory rates of this enzyme increased with increased concentrations of the *C. fusca* extract as follows: 35 μg mL^{-1}; 54% → 70 μg mL^{-1}; 73% → 140 μg mL^{-1}; 93% (Fig. 2A). Moreover, the present data showed similar patterns to the results of DPPH and ABTS radical scavenging assays. These symptoms may be strongly associated with the fatty acid profiles and contents of *C. fusca*, as reported in previous studies (Ando et al. 2004, Zhou et al. 2022, 2023, Ferdous et al. 2023, Kang et al. 2023). Even though the methanol extracts were detected to have approximately 20% lower inhibition abilities compared to the positive control (ascorbic acid, 96% at 70 μg mL^{-1}), this material may be considered an outstanding natural functional food agent beneficial to humans owing to its diverse metabolites and biological properties. To gather further information on these tyrosinase inhibitory properties, we investigated the inhibition patterns at the reaction times during 30 min. When the reaction time was increased (0 → 30 min, 2 min intervals), the inhibition rates of extracts at differ-

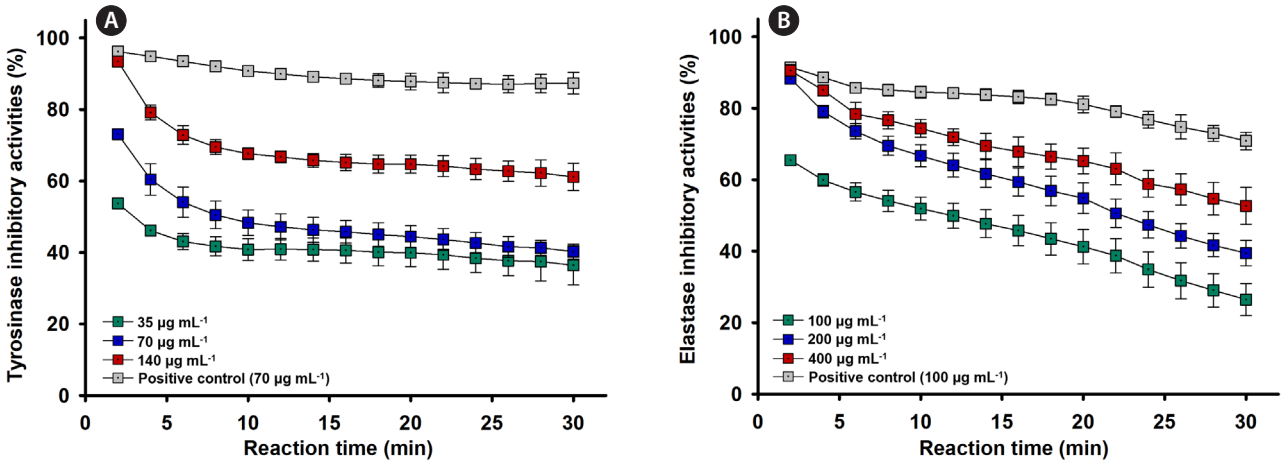

Fig. 2. Comparisons of tyrosinase and elastase inhibitory capacities in the methanol extracts of *Chlorella fusca* through reaction times. (A) Tyrosinase inhibitory effects. (B) Elastase inhibitory effects.

ent concentrations decreased in a dose-dependent manner (Fig. 2A). To be specific, according to the increases of reaction times at 140 μg mL^{-1}, the tyrosinase inhibitory activities were reduced by 93% (2 min) → 79% (4 min) → 73% (6 min) → 70% (8 min) → 67% (12 min) → 65% (20 min) → 63% (24 min) → 61% (30 min), compared to those of the positive control (96 → 87%, 70 μg mL^{-1}). Furthermore, other concentrations exhibited similar tendencies with 73% (2 min) → 60% (4 min) → 48% (10 min) → 45% (18 min) → 40% (30 min) at 70 μg mL^{-1} and 54% (2 min) → 46% (4 min) → 41% (10 min) → 40% (18 min) → 36% (30 min) at 35 μg mL^{-1}. Notably, the inhibition effects of this enzyme considerably decreased up to 0 → 10 min, and the reaction times between 10 and 30 min showed mild variations with slight decreases. These findings indicate that *C. fusca* may be considered an effective agent for skin-whitening in the cosmetic industry (Ando et al. 2004, Safarfar et al. 2015, Ferdous et al. 2023). In addition, it is believed that *C. fusca* extract will help promote potential applications in crop growth, such as flowering, cultivation, seedling development, resistance to environmental stress, and various human health-promoting abilities, as previously described (Musharraf et al. 2012, Safi et al. 2014, Kotrbácek et al. 2015, Deamici et al. 2019, EI-fayoumy et al. 2021, Martini et al. 2021, Canelli et al. 2022, Ferdous et al. 2023).

Another study on cosmeceutical functions was conducted on elastase inhibitory activity. According to the precedent experimental results of antioxidant and tyrosinase inhibitory activities, the elastase inhibition patterns were measured with percentage ratios by comparing different concentrations of the sample and the positive control (ursolic acid). Their inhibitory properties increased with increasing concentrations of the sample as follows: 1,000 μg mL^{-1}, 100%; 500 μg mL^{-1}, 100%; 400 μg mL^{-1}, 91%; and 200 μg mL^{-1}, 88%. Although 100% inhibition was detected at 1,000 and 500 μg mL^{-1}, the elastase inhibition rate was evaluated at 400 μg mL^{-1} owing to dose-dependent variation. Elastase inhibition was 3-fold lower compared to that of tyrosinase (Fig. 2). These observations suggest that the metabolite profiles and contents, such as fatty acids, of the *C. fusca* extract may lead to higher effective inhibitory capacities for tyrosinase than elastase, as shown in earlier studies (Ando et al. 2004, Zhou et al. 2022). This phenomenon was also similar to that reported in previous research on the anti-elastase and anti-tyrosinase abilities of earthworm extracts (Azmi et al. 2014). As shown in Fig. 2B, considerable differences in the elastase inhibition patterns were observed at three different concentrations of 400, 200, and 100 μg mL^{-1} with the rank order as follows: 91 > 88 > 66%. Even though the *C. fusca* extract showed mildly lower inhibitory abilities than the positive control (92% at 100 μg mL^{-1}), this material may be a potent anti-elastase source for improving skin elasticity and resistance. To obtain more information on the variation trends under different reaction times, the methanol extract was examined for elastase inhibitory capacities during 30 min (2 min intervals) at different concentrations (Fig. 2B). Briefly, the elastase inhibitory rates persistently decreased with increasing reaction time, with significant differences depending on concentration. Especially, the inhibition patterns of this enzyme were remarkably different from those of tyrosinase. For example, the *C. fusca* extract at 400 μg mL^{-1} was considerably reduced by 92%; 2 min → 53%; 30 min when the increase of reaction times (92%; 2 min → 74%; 10 min → 65%; 20 min → 53%; 30

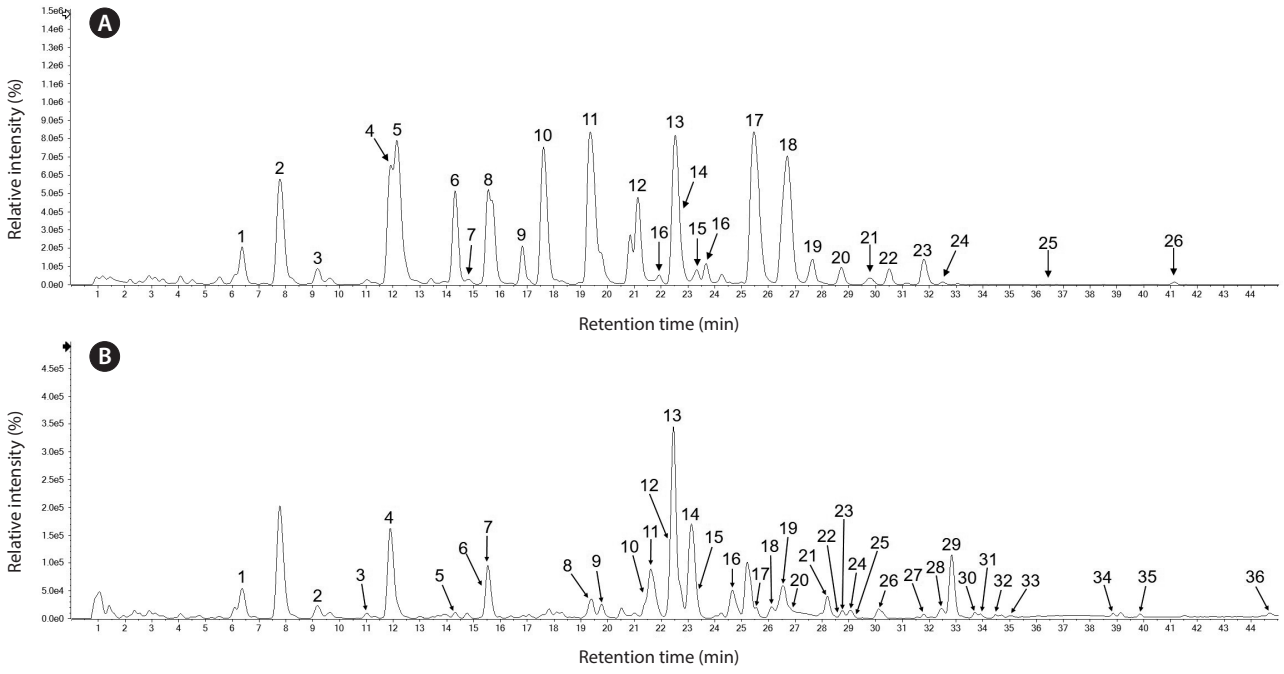

Fig. 3. Ultra-high performance liquid chromatography coupled with quadrupole time-of-flight mass spectrometry (UPLC-Q-TOF-MS/MS) base peak intensity chromatograms through different ion modes in the methanol extract of *Chlorella fusca*. (A) UPLC-Q-TOF-MS chromatogram using negative ion mode. (B) UPLC-Q-TOF/MS chromatogram using positive ion mode.

min) and showed the continuous decrease patterns (88%; 2 min → 67%; 10 min → 55%; 20 min → 39%; 30 min) with dose-dependent capacities at 200 μg mL^{-1}. The positive control (100 μg mL^{-1}) also displayed similar tendencies (92%; 2 min → 85%; 10 min → 81%; 20 min → 71%; 30 min), specifically, their inhibition rates were seen to have an approximately 30% higher effect when compared to the sample extracts (Fig. 2B). These results imply that the inhibitory capacities of the samples against elastase may be positively related to the presence and content of abundant metabolites (Ando et al. 2004, Zhou et al. 2022, 2023, Kang et al. 2023). For the above considerations, *C. fusca* extract may be used as a potent cosmeceutical agent and an excellent natural source for the anti-aging industry. As far as we know, the present research is the first to evaluate the inhibition activities of *C. fusca*, including those against tyrosinase and elastase.

Elucidation of metabolite profiles in *Chlorella fusca* extract using negative and positive ion modes of UPLC-Q-TOF-MS/MS

UPLC coupled with mass spectrometric detection has been widely used to investigate metabolite profiles with molecular weights in diverse natural sources, such as crops, foods, and vegetables (Rivera et al. 2014, Pantami et al. 2020, Koch et al. 2021, Feng et al. 2022). This technique offers the most meaningful information for characterization through metabolite assignment, which involves the fragmentation of a selected precursor ion in the product ions from the various peaks of the target sample (Nilsson et al. 2010, Rivera et al. 2014, Koch et al. 2021). For these reasons, to obtain exact information on the metabolite profiles of *C. fusca*, UPLC-Q-TOF-MS/MS analysis was carried out in both negative and positive ion modes. Moreover, we used a highly polar methanol solvent to achieve an effective metabolite extraction ratio (Safarfar et al. 2015, Zhou et al. 2022, Ferdous et al. 2023, Lee et al. 2023). The metabolite constituents were tentatively elucidated by comparing the product ions and their selected precursor ions to the MS and MS/MS data of the detected peaks in previous studies on *Chlorella* species as well as the phytochemical dictionary, Massbank (https://www.Massbank.jp), and ChemSpider (https://www.chemspider.com) of the Natural Products Database. In the current study, a complete chromatographic separation of many metabolites, including major and minor peaks was achieved within 45 min (Fig. 3).

First, we demonstrated 26 components in diverse peaks by the negative ion mode from the methanol extract of *C. fusca* (Fig. 3A). Their structures were identified with five chemical skeletons: 4-nonylphenol, diterpene

alcohol, fatty alcohol, fatty acid, and chlorophyll groups (Fig. 4A). The TOF-MS and MS/MS analyses of peak 1 (t_R = 6.3 min) presented the molecular ion $[M–H]^-$ at *m/z* 293.2134 (1A in Supplementary Fig. S2A) and a fragment ion at *m/z* 195.1378 (1B in Supplementary Fig. S2A), which was formed by the loss of the *m/z* 98 fragment (cleavage of hydroxybenzene ring: 68 amu; $C_4H_4O^-$ and methoxy group: 30 amu; OCH_3^-). Based on the above molecular ions and previous data, this peak was elucidated as 4-nonyl-(1-methyl, 6,8-methoxy)-hydroxybenzene (**1**) of the 4-nonylphenol group (López-Pacheco et al. 2019). The UPLC-TOF-MS/MS scan of peak 2 (t_R = 7.7 min) exhibited an identical molecular ion $[M–H]^-$ at *m/z* 295.2283 and the two fragment ions at *m/z* 167.1076 and *m/z* 141.1279 (2A and 2B in Supplementary Fig. S2A). These ions were characterized as phytol (**2**), in agreement with previous work on *C. vulgaris* axenic culture (El-fayoumy et al. 2021). The product ions mass spectra of peaks 3 (t_R = 9.1 min) and 4 (t_R = 11.9 min) displayed $[M–H]^-$ ions at *m/z* 295.2293 and *m/z* 297.2439, respectively, and their characteristic fragment ions were observed at *m/z* 195.1377 and *m/z* 185.1163 in the MS/MS analysis (3A, 4A, 3B, and 4B in Supplementary Fig. S2A). Especially, these fragment ions were formed by the losses of *m/z* 100 amu {$[M–H]^-$–[-CH-$(CH_2)_5OH]^-$; 195 amu} and *m/z* 112 amu {$[M–H]^-$–[-CH-$(CH_2)_6CH_3]^-$; 185 amu}. The above molecular weights and fragmentation patterns were similar to those of fatty acids in the published literature (Nilsson et al. 2010). According to the summarized ions and *Chlorella* research information, peaks 3 and 4 were identified as 11-eicosenol (**3**) and 1-eicosanol (**4**), which are fatty alcohol derivatives (Fernandes and Cordeiro 2020). The abundant metabolite types in the remaining diverse peaks were identified as fatty acids and chlorophyll compositions, based on the characteristics of molecular ions and data from earlier studies. Their peaks were as follows: fatty acids, eight peaks 5, 6, 8, 10–12, 17, and 18; chlorophyll, one peak 13 (Figs 3A & 4A). Peak 5 (t_R = 12.1 min) exhibited an identical molecular ion $[M–H]^-$ at *m/z* 247.1708 and three major fragment ions at *m/z* 203.1793, *m/z* 175.1480, and *m/z* 149.1328 (5A and 5B in Supplementary Fig. S2A). Three fragment ions were assigned as lipid residues with a loss of *m/z* 44 {$[M–H]^-$–44 amu ($–COO^-$); *m/z* 203}, *m/z* 72 {([M–H]$^-$–72 amu ($–CH_2$-CH_2-COO^-); *m/z* 175)}, and *m/z* 98 {([M–H]$^-$–98 amu (–CH-CH-CH_2-CH_2-$COOH^-$); *m/z* 149)} (Stigter et al. 2013). According to the above ion profile, this peak coincides with those of hexadeca-4,7,10,13-tetraenoic acid in high concentrations of algae and fish oil (Stigter et al. 2013). The deprotonated molecular ion $[M–H]^-$ at *m/z* 249.1863 was found in the UPLC-TOF-MS spectrum of peak 6 (t_R = 14.2 min) and two fragments (*m/z* 205.1950 and *m/z* 177.1644) were produced in MS/MS data (6A and 6B in Supplementary Fig. S2A). The precursor ion at *m/z* 205.1950 resulted from the loss of the carboxylic acid ($–COO^-$: 44 amu) moiety, and the fragmentation ion at *m/z* 177.1644 was formed by the loss of the $–CH_2$-CH_2-COO^- (72 amu) (Stigter et al. 2013). These fragmentation characteristics were consistent with those of peak 5. As a result, peak 6 was tentatively assigned to roughanic acid (**6**) based on a previous report (Cholewski et al. 2018). The TOF-MS and MS/MS spectra of peak 8 (t_R = 15.5 min) displayed a $[M–H]^-$ ion at *m/z* 299.2596 and two fragment ions at *m/z* 185.1168 and *m/z* 139.1123 (8A and 8B in Supplementary Fig. S2A). In particular, these fragment ions may be related to the typical characteristics of cleavage residues in fatty acid structures, as observed in the patterns of peaks 3–5. Moreover, the ion patterns of this peak were in agreement with those of fatty acid derivatives in microalgae sources (Musharraf et al. 2012). Based on this evidence, peak 8 was assumed to be 10-hydroxyoctadecanoic acid (**8**) (Musharraf et al. 2012). The negative ion mode of peak 9 (t_R = 16.8 min) exhibited a molecular ion at *m/z* 275.2024 (MS) and a fragment ion at *m/z* 231.2095 (MS/MS) through the loss of a carboxylic acid moiety (44 amu, $–COO^-$) (9A and 9B in Supplementary Fig. S2A). The above ion patterns were similar to those of peak 6 and coincided with the chemical characteristics of fatty lipids in *C. pyrenoidosa* among *Chlorella* species (Montes D'Oca et al. 2011). Therefore, peak 9 was tentatively confirmed as stearidonic acid (**9**). Full mass scan analyses of peaks 10 (t_R = 17.6 min) and 14 (t_R = 22.6 min) were detected with $[M–H]^-$ ions at *m/z* 251.2018 and *m/z* 279.2327 (10A and 14A in Supplementary Fig. S2A) and their fragment ions at *m/z* 233.1894 and *m/z* 261.2211 (10B and 14B in Supplementary Fig. S2A). The precursor ions were attributed to the losses of hydrogen ions (–18 amu), including the hydroxyl moiety, and were in agreement with the patterns of fatty acids in *C. sorokiniana* and *C. vulgaris* (Yun et al. 2020, Gorgich et al. 2021). By comparing their mass values with data reported in an earlier study, the two peaks were tentatively demonstrated as 7,10-hexadecadienoic acid (**10**) and linoleic acid (**14**) (Pantami et al. 2020). Full TOF-MS in negative ion mode of peak 11 (t_R = 19.3 min) exhibited a molecular ion at *m/z* 277.2174 and the MS/MS spectrum showed two minor fragment ions (*m/z* 233.2265 and *m/z* 219.1392) (11A and 11B in Supplementary Fig. S2A). Their fragment ions resulted from the losses of 44 amu (carboxyl moiety: $–COO^-$) and 58 amu (methyl carboxyl moiety: $–CH_2$-COO^-), as indicated by

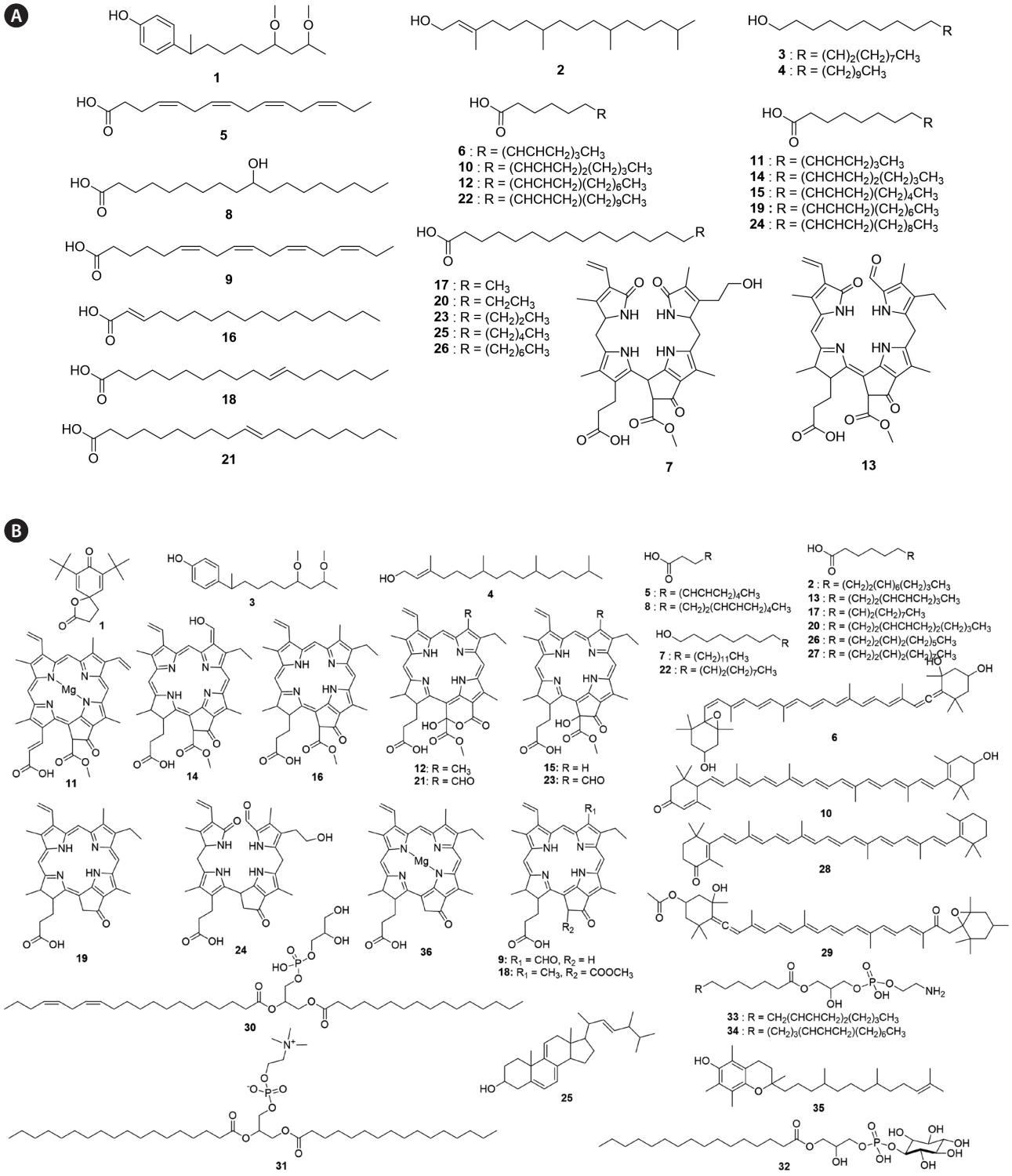

Fig. 4. Chemical structures of the identified metabolite compositions from the methanol extract of *Chlorella fusca*. (A) Metabolite structures through negative ion mode of ultra-high performance liquid chromatography coupled with quadrupole time-of-flight mass spectrometry (UPLC-Q-TOF-MS/MS). (B) Metabolite structures through positive ion mode of UPLC-Q-TOF-MS.

previous results related to the rapid quantification of fatty acids in plants using high-performance liquid chromatography mass spectrometry (Pantami et al. 2020, Koch et al. 2021). On the basis of the above mass patterns and molecular weights of published data, this peak was documented as α-linolenic acid (**11**) (Shimma et al. 2012, Yun et al. 2020, Koch et al. 2021). Subsequently, 13 peaks, 12 and 15–26, were identified by comparisons with the exact MS and MS/MS values using UPLC coupled with the TOF-mass technique, as well as previous results. Their peaks were also compared with the retention times in the chromatogram, in accordance with an earlier study. In the current work, the deprotonated molecular ions were found as follows: *m/z* 253.2177 (**12**), *m/z* 253.2184 (**15**), *m/z* 267.2338 (**16**), *m/z* 255.2327 (**17**), *m/z* 281.2483 (**18**), *m/z* 281.2493 (**19**), *m/z* 269.2497 (**20**), *m/z* 295.2649 (**21**), *m/z* 295.2649 (**22**), *m/z* 283.2647 (**23**), *m/z* 309.2803 (**24**), *m/z* 311.2960 (**25**), and *m/z* 339.3269 (**26**) (12A, 15A–26A, 12B, and 15B–26B in Supplementary Fig. S2A). According to the above investigation, their metabolites were tentatively assigned fatty acid distributions, as detailed below (Table 1): 7-hexadecenoic acid (**12**) (t_R = 21.1 min), palmitoleic acid (**15**) (t_R = 23.3 min), heptadecenoic acid (**16**) (t_R = 23.6 min), palmitic acid (**17**) (t_R = 25.4 min), vaccenic acid (**18**) (t_R = 26.7 min), oleic acid (**19**) (t_R = 27.6 min), heptadecanoic acid (**20**) (t_R = 28.6 min), 10-nonadecenoic acid (**21**) (t_R = 29.7 min), 7-nonadecenoic acid (**22**) (t_R = 30.5 min), stearic acid (**23**) (t_R = 31.8 min), gadoleic acid (**24**) (t_R = 32.4 min), arachidic acid (**25**) (t_R = 36.3 min), and behenic acid (**26**) (t_R = 41.1 min) (Montes D'Oca et al. 2011, Yun et al. 2020, Gorgich et al. 2021, Koch et al. 2021). The remaining minor one major peaks (7 and 13) in the negative ion mode showed deprotonated ions $[M–H]^-$ at *m/z* 631.2390 and *m/z* 625.2603 (7A and 13A in Supplementary Fig. S2A), as well as various fragment ions (peak 7: *m/z* 553.2063; peak 13: *m/z* 581.2700, *m/z* 565.2384, *m/z* 538.2510, and *m/z* 521.2497) (7B and 13B in Supplementary Fig. S2A). The MS/MS fragmentation of the ion at *m/z* 553.2063 in peak 7 may be related to loss of the hydroxymethyl (or methoxy) moiety. Among the diverse fragment ions of peak 13, the distinctive product ion at *m/z* 581.2700 ($[M–H]^-$–44 amu) corresponded to the loss of a carboxylic acid moiety, and the fragment ion at *m/z* 565.2384 resulted from the loss of an acetate moiety ($[M–H]^-$–CH_3COO^-: 60 amu). Also, the fragmentation at *m/z* 521.2497 ($[M–H]^-$–104 amu) exhibited losses of carboxylic (44 amu) and acetate (60 amu) moieties. These two peaks were achieved by comparing the molecular weights obtained in the current work with previously reported data concerning chlorophyll derivatives in grapevine and basil leaves (Li et al. 2018, Moser et al. 2020). In particular, a previous study documented that peak 13 is converted to peak 7 via the pheophorbide oxygenase / phyllobilin pathway for chlorophyll breakdown (Moser et al. 2020). Based on the above considerations, their chemical structures were determined to chlorophyll catabolite (phyllobilin) (**7**) and 10,22-dihydro-4,5-dioxo-4,5-seco-pheophorbide a (**13**). Although two compositions have been previously identified in other natural materials, we demonstrated for the first time their presence in *Chlorella* source. Overall, we revealed 26 metabolites, including one 4-nonylphenol (**1**), one diterpene alcohol (**2**), two fatty alcohols (**3** and **4**), two chlorophylls (**7** and **13**), and 20 fatty acids (**5**, **6**, **8**–**12**, and **14**–**26**) in the negative ion mode using the UPLC-TOF-MS/MS technique from the methanol extract of *C. fusca* (Fig. 4A).

To obtain more valuable information on the metabolite profiles of *C. fusca*, we also conducted analyses in the positive ion mode of UPLC-TOF-MS. As illustrated in Fig. 3B, the complete chromatographic separation of various metabolites was achieved within 45 min. A total of 36 metabolites were tentatively identified, and their structures were confirmed to belong to 11 chemical groups: fatty acid, fatty alcohol, chlorophyll, carotenoid, lysophospholipid, lipid, oxaspiro, 4-nonylphenol, diterpene alcohol, ergostane, and tocopherol (Fig. 4B). Among the various metabolites, 10 compositions were identified by the full scan experiment in the negative ion mode (peaks 3–5, 7, 8, 13, 17, 20, 26, and 27) (Table 1). In particular, peaks 4, 13, and 14 exhibited remarkably higher intensities than the other components (Fig. 3B). Peak 1 (t_R = 6.3 min) showed a molecular ion $[M+H]^+$ at *m/z* 277.2153, and the MS/MS fragmentation patterns exhibited three major and three minor fragment ions at *m/z* 189.1259, *m/z* 159.1178, *m/z* 147.1176, and *m/z* 107.0856 (1A and 1B in Supplementary Fig. S2B). Based on these molecular ions, this compound was tentatively identified as 7,9-di-tert-butyl-1-oxaspiro[4.5]deca-6,9-diene-2,8-dione (**1**) by comparison with previously reported data on *Chlorella* species and mass spectra in the NIST Chemistry WebBook. The TOF-MS analysis of peak 2 (t_R = 9.1 min) revealed the molecular ion $[M+H]^+$ at *m/z* 279.2307 (2A in Supplementary Fig. S2B) and fragment ions in the MS/MS spectrum were observed at *m/z* 149.0247, *m/z* 121.1024, and *m/z* 107.0863 (2B in Supplementary Fig. S2B). These ion patterns are similar to those of peaks 5, 6, and 11, due to the losses of various –CH_2-COOH moieties (–130 amu, –158 amu, –170 amu, and –172 amu). In addition, their patterns were based on earlier studies of commercial *C. vulgaris* and cultivated microalgae (Sotou-

Table 1. Identification of metabolite profiles in the methanol extract of *Chlorella fusca* by the negative and positive ion modes of UPLC-Q-TOF-MS/MS

Peak	t_R (min)	Formula	Calculated mass [M] (*m/z*)	Calculated mass $[M-H]^-$ (*m/z*)	Observed molecular ion in MS $[M-H]^-$ (*m/z*)	Observed fragment ions in MS^2 (*m/z*)	Error (MS)	Error (MS^2)	Identification
Negative ion mode									
1	6.3	$C_{18}H_{30}O_3$	294.2195	293.2117	293.2134	293.2098 / 195.1378	1.6	-	4-Nonyl-(1-methyl, 6,8-metoxy)-hydroxybenzene
2	7.7	$C_{20}H_{40}O$	296.3079	295.3001	295.2283	295.2254 / 167.1076 / 141.1279	-	-	Phytol
3	9.1	$C_{20}H_{40}O$	296.3079	295.3001	295.2293	295.2255 / 195.1377	1.5	4.2	11-Eicosenol
4	11.9	$C_{20}H_{42}O$	298.3236	297.3157	297.2439	297.2407 / 185.1163	-	-	1-Eicosanol
5	12.1	$C_{16}H_{24}O_2$	248.1776	247.1698	247.1708	247.1690 / 203.1793 / 175.1480 / 149.1328	2.8	1.7	Hexadeca-4,7,10,13-tetraenoic acid
6	14.2	$C_{16}H_{26}O_2$	250.1933	249.1855	249.1863	249.1837 / 205.1950 / 177.1644	0.8	1.3	Roughanic acid
7	14.7	$C_{34}H_{40}N_4O_8$	632.2846	631.2768	631.2390	613.2270 / 553.2063	1.7	3.8	Chlorophyll catabolites (phyllobilin)
8	15.5	$C_{18}H_{36}O_3$	300.2664	299.2586	299.2596	299.2567 / 185.1168 / 139.1123	1.3	2.4	10-Hydroxyoctadecanoic acid
9	16.8	$C_{18}H_{28}O_2$	276.2089	275.2011	275.2024	275.1994 / 231.2095	0	0.5	Stearidonic acid
10	17.6	$C_{16}H_{28}O_2$	252.2089	251.2011	251.2018	251.1991 / 233.1894 / 106.0425	1.3	3.2	7,10-Hexadecadienoic acid
11	19.3	$C_{18}H_{30}O_2$	278.2246	277.2168	277.2174	277.2150 / 233.2265 / 219.1392	0.1	1.8	Linolenic acid
12	21.1	$C_{16}H_{30}O_2$	254.2246	253.2168	253.2177	253.2143	0.3	3.4	7-Hexadecenoic acid
13	22.4	$C_{35}H_{38}N_4O_7$	626.2740	625.2662	625.2603	625.2582 / 581.2700 / 521.2497	1.8	0	10,22-Dihydro-4,5-dioxo-4,5-secopheophorbide a
14	22.6	$C_{18}H_{32}O_2$	280.2402	279.2324	279.2327	279.2307 / 261.2211	1.2	2.4	Linoleic acid
15	23.3	$C_{16}H_{30}O_2$	254.2246	253.2168	253.2184	253.2212	0.7	4.8	Palmitoleic acid
16	23.6	$C_{17}H_{32}O_2$	268.2402	267.2324	267.2338	267.2300	4.4	0	Heptadecenoic acid
17	25.4	$C_{16}H_{32}O_2$	256.2402	255.2324	255.2327	255.2299	0.9	2.7	Palmitic acid
18	26.7	$C_{18}H_{34}O_2$	282.2559	281.2481	281.2483	281.2455	1.1	3.8	Vaccenic acid
19	27.6	$C_{18}H_{34}O_2$	282.2559	281.2481	281.2493	281.2455	2.5	0	Oleic acid
20	28.6	$C_{17}H_{34}O_2$	270.2559	269.2481	269.2497	269.2456	4.0	4.9	Heptadecanoic acid
21	29.7	$C_{19}H_{36}O_2$	296.2715	295.2637	295.2649	295.2612	2.3	0	10-Nonadecenoic acid
22	30.5	$C_{19}H_{36}O_2$	296.2715	295.2637	295.2649	295.2612	2.1	2.7	7-Nonadecenoic acid
23	31.8	$C_{18}H_{36}O_2$	284.2715	283.2637	283.2647	283.2607	1.4	0	Stearic acid
24	32.4	$C_{20}H_{38}O_2$	310.2872	309.2794	309.2803	309.2772	1.2	0	Gadoleic acid
25	36.3	$C_{20}H_{40}O_2$	312.3028	311.2950	311.2960	311.2930	1.4	0	Arachidic acid
26	41.1	$C_{22}H_{44}O_2$	340.3341	339.3263	339.3269	339.3243	0.2	3.7	Behenic acid
Positive ion mode									
1	6.3	$C_{17}H_{24}O_3$	276.1725	277.1803	277.2153	189.1259 / 159.1178 / 147.1176 / 107.0856	2.2	2.6	7,9-Di-tert-butyl-1-oxaspiro[4.5] deca-6,9-diene-2,8-dione
2	9.1	$C_{18}H_{30}O_2$	278.2245	279.2324	279.2307	149.0247 / 121.1024 / 109.1018 / 107.0863	1.6	0	α-Eleostearic acid
3	11.0	$C_{18}H_{30}O_3$	294.2194	295.2273	295.2257	163.1139 / 131.0868 / 121.1021	2.8	1.7	4-Nonyl-(1-methyl, 6,8-metoxy)-hydroxybenzene
4	11.9	$C_{20}H_{40}O$	296.3079	297.3157	297.2439	297.2407 / 279.2312 / 185.1163	-	-	Phytol
5	14.2	$C_{16}H_{24}O_2$	248.1776	249.2218	249.1863	249.1837 / 231.1748 / 177.1644 / 175.1494	1.2	2.7	Hexadeca-4,7,10,13-tetraenoic acid

Table 1. Continued

Peak	t_R (min)	Formula	Calculated mass [M] (*m/z*)	Calculated mass [M-H]$^-$ (*m/z*)	Observed molecular ion in MS [M-H]$^-$ (*m/z*)	Observed fragment ions in MS^2 (*m/z*)	Error (MS)	Error (MS^2)	Identification
6	15.5	$C_{40}H_{56}O_4$	600.4178	601.4256	601.5371	283.2610 / 247.2399	2.5	1.7	Neoxanthin
7	15.6	$C_{20}H_{42}O$	298.3235	299.3313	299.2596	299.2567 / 281.2467 / 253.2522 / 141.1277	1.3	3.2	1-Eicosanol
8	19.3	$C_{18}H_{28}O_2$	276.2089	277.2167	277.2174	277.2150 / 259.2058	0.3	1.2	Stearidonic acid
9	19.6	$C_{33}H_{32}N_4O_4$	548.2423	549.2501	549.2484	549.2471 / 521.2545	0.3	4.5	Pyropheophorbide b
10	21.3	$C_{40}H_{54}O_2$	566.4123	567.4202	567.4166	567.4198 / 211.1488 / 145.1019 / 119.0862	1.2	2.4	3′-Oxolutein
11	21.6	$C_{35}H_{28}MgN_4O_5$	608.1910	609.1988	609.2676	609.2638 / 591.2548	0.7	4.8	Chlorophyll c2
12	22.4	$C_{35}H_{36}N_4O_7$	624.2584	625.2662	625.2603	625.2582 / 565.2384 / 521.2497	4.2	1.1	151-OH-Lactone-pheo a
13	22.6	$C_{18}H_{30}O_2$	278.2245	279.2324	279.2327	279.2307 / 261.2211	0.1	2.4	Linolenic acid
14	23.1	$C_{35}H_{34}N_4O_6$	606.2478	607.2556	607.2563	607.2538 / 575.2272 / 531.2371 / 487.2470	1.1	0.5	Pheophorbide b
15	23.3	$C_{35}H_{36}N_4O_6$	608.2634	609.2713	609.2665	609.2622 / 591.2527	1.1	0.6	132-OH-Pheo a
16	24.6	$C_{35}H_{36}N_4O_5$	592.2685	593.2764	593.2723	593.2687 / 533.2506	0.9	2.7	Pheide a
17	25.4	$C_{16}H_{30}O_2$	254.2245	255.2324	255.2327	255.2299 / 237.2217	0	1.5	7-Hexadecenoic acid
18	26.0	$C_{35}H_{36}N_4O_5$	592.2685	593.2764	593.2720	593.2691 / 533.2500	1.1	3.8	Pheophorbide a
19	26.5	$C_{33}H_{34}N_4O_3$	534.2630	535.2709	535.2668	535.2628 / 507.2716	0.8	2.2	Pyro-pheophorbide a
20	26.7	$C_{18}H_{32}O_2$	280.2402	281.2480	281.2483	281.2455 / 263.2370	0.2	2.2	Linoleic acid
21	28.1	$C_{35}H_{34}N_4O_8$	638.2376	639.2454	639.2766	639.2724 / 621.2643 / 579.2553 / 552.2671	4.0	4.9	151-OH-Lactone-pheo b
22	28.6	$C_{18}H_{36}O$	268.2766	269.2844	269.2497	269.2456 / 251.2368	1.0	1.5	9-Octadecen-1-ol
23	28.7	$C_{35}H_{34}N_4O_7$	622.2427	623.2505	623.2815	623.2803 / 605.2693 / 545.2488 / 546.2559	0.4	2.3	132-OH-pheo b
24	28.9	$C_{33}H_{38}N_4O_6$	586.2791	587.2869	587.4315	587.4295 / 569.4201 / 228.1369	0.2	4.2	Pyro-NCC 3
25	29.0	$C_{28}H_{42}O$	394.3235	395.3313	395.3280	395.3300 / 377.3202 / 211.1479 / 157.1019	0.7	2.2	9,11-Dehydroergosterol
26	30.1	$C_{16}H_{30}O_2$	254.2245	255.2324	255.2341	255.2317	4.6	5.0	Palmitoleic acid
27	31.8	$C_{18}H_{34}O_2$	282.2558	283.2637	283.2647	283.2607 / 265.2521	1.4	0	Oleic acid
28	32.4	$C_{40}H_{54}O$	550.4174	551.4252	551.4199	551.4245 / 211.1487 / 145.1020 / 119.0858	1.5	1.7	Echinenone
29	32.8	$C_{43}H_{60}O_5$	656.4440	657.4519	657.4106	657.4068 / 597.3844	0.6	3.0	All-trans fucoxanthin
30	33.6	$C_{44}H_{83}O_{10}P$	802.5723	803.5802	803.4916	803.5121 / 277.2159 / 179.0590	0.5	3.3	PG (16:0/22:2)
31	33.8	$C_{42}H_{84}NO_8P$	761.5934	762.6012	762.5092	565.4235 / 335.2551	0.4	1.2	PC (16:0/18:0)
32	34.4	$C_{25}H_{49}O_{12}P$	572.2961	573.3039	573.4508	573.4489 / 296.2290 / 185.1172	1.9	2.9	PI (16:0/0:0)
33	34.9	$C_{23}H_{44}NO_7P$	477.2855	478.2933	478.3853	460.3771 / 222.1478 / 140.0712	1.8	0	LPE (18:2/0:0)
34	38.9	$C_{25}H_{50}NO_7P$	507.3324	508.3403	508.5064	508.5074 / 146.1181	1.7	0	LPE (20:1/0:0)
35	39.8	$C_{29}H_{48}O_2$	428.3654	429.3732	429.3693	429.3169 / 165.0908 / 149.0963	1.3	2.4	11'-α-tocomonoenol
36	44.7	$C_{33}H_{32}MgN_4O_3$	556.2324	557.2403	557.4560	557.4531 / 279.2312	2.1	3.2	Pyrochlorophyllide a

UPLC-Q-TOF-MS/MS, ultra-high performance liquid chromatography coupled with quadrupole time-of-flight mass spectrometry; PG, phosphatidylglycerol; PC, phosphatidylglycerol; PI, phosphatidylinositol; LPE, lysophophatidylethanolamine.

dehniakarani et al. 2019). Thus, this peak was confirmed as α-eleostearic acid (**2**). Full TOF mass analyses of peaks 6, 10, 28, and 29 were observed for $[M+H]^+$ ions at *m/z* 601.5371, *m/z* 567.4166, *m/z* 551.4199, and *m/z* 657.4106, and their retention times were 15.5, 21.3, 32.4, and 32.8 min, respectively. Fragment ions were detected in the MS/MS spectra, as illustrated in Table 1. Especially, the characteristic MS/MS fragment ion at *m/z* 283.2610 of peak 6 resulted from the loss of water (H_2O) and $C_{20}H_{27}O$ residue in the protonated parent ions (6A and 6B in Supplementary Fig. S2B). This may indicate an α-cleavage of the molecular following a radical side rearrangement through π-bond dissociation of the molecular ion (Pantami et al. 2020). Based on the above ion patterns and earlier results for carotenoid derivatives, this peak was assigned to neoxanthin (**6**) (Rivera et al. 2014, Pantami et al. 2020). In the TOF-MS and MS/MS spectra, peak 10 was detected as a protonated ion $[M+H]^+$ at *m/z* 567.4166 with three signals at *m/z* 211.1488 ($[M+H]^+$–356 amu), *m/z* 145.1019 ($[M+H]^+$–422 amu), and *m/z* 119.0862 ($[M+H]^+$ –448 amu) (10A and 10B in Supplementary Fig. S2B). Three ion peaks indicate the presence of conjugated polyene chains with cleavage of characteristic fragmentations regarding the 3'-keto chromophoric moiety of the β-end group and the 3-hydroxy furanoid moiety of the ε-end group (Molnár et al. 2006) in the carotenoid structures, as previously published (Rivera et al. 2014, Pantami et al. 2020). From the mentioned evidence, this peak was characterized as 3'-oxolutein with the $C_{40}H_{54}O_2$ formula. The patterns of fragmentation ions in peaks 28 and 29 were similar to those of the carotenoid derivatives **6** and **10** (28A, 28B and 29A, 29B in Supplementary Fig. S2B). The fragment ions were assigned as residues (peak 28: *m/z* 211.1487, *m/z* 145.1020, and *m/z* 119.0858) through the cleavage of mono keto furanoid and furanoid frameworks (Rivera et al. 2014, Pantami et al. 2020), and two fragment ions at *m/z* 597.3884 and *m/z* 581.3959 in peak 29 were characterized as carotenoid residues due to the losses of the acetate ion (CH_3COO^-, 60 amu) and CH_3COO^-+OH^-, 76 amu) (Stigter et al. 2013). Based on the above molecular weights and previous results, peaks 28 and 29 were identified as echinenone (**29**) and all-trans fucoxanthin (**30**). Subsequently, 12 peaks (9, 11, 12, 14–16, 18, 19, 21, 23, 24, and 36) exhibited the molecular ions ($[M+H]^+$) at *m/z* 549.2484, *m/z* 609.2676, *m/z* 625.2603, *m/z* 607.2563, *m/z* 609.2665, *m/z* 593.2723, *m/z* 593.2720, *m/z* 535.2668, *m/z* 639.2766, *m/z* 623.2815, *m/z* 587.4315, and *m/z* 557.4560 (Table 1, Supplementary Fig. S2B). Furthermore, their main product ions in the TOF-MS/MS chromatograms are displayed as follows: *m/z* 521.2545 (**9**), *m/z* 591.2548 (**11**), *m/z* 581.2700, 565.2384, 538.2510, and 521.2497 (**12**), *m/z* 531.2371 (**14**), *m/z* 591.2327, 559.2282, 531.2300, and 515.2406 (**15**), *m/z* 533.2506 (**16**), *m/z* 533.2500 (**18**), *m/z* 507.2716 (**19**), *m/z* 621.2643, 579.2553, and 552.2671 (**21**), *m/z* 605.2693 and 545.2488 (**23**), *m/z* 309.2054 (**24**), and *m/z* 279.2312 (**36**). Most of the fragment ions resulted from the losses of methyl, hydroxyl, acetyl, CO, and their mixed moieties, as earlier studies have determined for chlorophyll derivatives in natural plants (Li et al. 2018, Viera et al. 2018). Additionally, these 12 peaks exhibited similar patterns to those of chlorophyll structures (Chen et al. 2015*a*, 2015*b*, Li et al. 2018, Viera et al. 2018). Their chemical structures are listed in Table 1 and shown in Fig. 4. To the best of our knowledge, little information has been obtained previously regarding the exact MS and MS/MS values of chlorophyll profiles in *C. fusca* by UPLC coupled with TOF-MS skill. To obtain more information on the metabolic components of the remaining peaks, we evaluated five peaks (30–34) within the range of 33.5–39.0 min (Fig. 3B). Previous studies have shown that many polar lipid profiles, such as phospholipids and glycolipids, are present in microalgal sources (Vello et al. 2018, Conde et al. 2021, Canelli et al. 2022). Especially, it is well demonstrated that the polar lipid compositions (phosphatidylcholine [PC], phosphatidylglycerol [PG], phosphatidylinositol [PI], lysophosphatidylethanolamine [LPE], lysophosphatidylcholine, and phosphatidylethanolamine) in *Chlorococcum amblystomatic* of green microalgae are known to exhibit health benefits of antioxidant and anti-inflammatory properties (Conde et al. 2021). A full TOF mass scan of five peaks (**30**; t_R = 33.6 min, **31**; t_R = 33.8 min, **32**; t_R = 34.4 min, **33**; t_R = 34.9 min, and **34**; t_R = 38.9 min) displayed the molecular ion $[M+H]^+$ at *m/z* 803.4916 (**30**), *m/z* 762.5092 (**31**), *m/z* 573.4508 (**32**), *m/z* 478.3853 (**33**), and *m/z* 508.5064 (**34**) (30A–34A in Supplementary Fig. S2B), and their fragment ions were as follows: *m/z* 513.3036 and *m/z* 277.2159 (**30**); *m/z* 335.2551 (**31**); *m/z* 295.2261 and *m/z* 185.1172 (**32**); *m/z* 222.1478 and *m/z* 140.0712 (**33**); *m/z* 146.1181 (**34**) (30B–34B in Supplementary Fig. S2B). Although the distribution of polar lipids displayed mild differences, our data are similar to those of earlier studies that determined the polar lipid components in microalgal species (Conde et al. 2021). Based on the fragmentation patterns in the published studies and their MS and MS/MS data in the present work, the chemical structures were elucidated as below: PG (16:0/22:2) (**30**), PC (16:0/18:0) (**31**), PI (16:0/0:0) (**32**), LPE (18:2/0:0) (**33**), and LPE (20:1/0:0) (**34**) (Shimma et al. 2012, Calvano et al. 2020, Conde et al. 2021). Peak 22 (t_R = 28.6 min) presented a

molecular ion ($[M+H]^+$) at *m/z* 269.2497 in the TOF-MS spectrum, and its characteristic fragment ion was *m/z* 251.2368 (22A and 22B in Supplementary Fig. S2B). This fragmentation pattern may result from the loss of a water or hydroxyl moiety ($[M+H-18, -18\ amu]^+$), which is in accordance with an earlier study (Rivera et al. 2014). The fragment pattern of this peak (*m/z* 269.2497 → *m/z* 251.2368) was also coincident with it of peak 27 (*m/z* 283.2647 → *m/z* 265.2521, oleic acid) through the loss of –18 amu. These ions were verified to have the same patterns as the metabolites in *C. stigmatophora* based on published data (Fernandes and Cordeiro 2020) and the mass spectrum in the NIST Chemistry WebBook. This component was confirmed to be 9-octadecen-1-ol (**22**) and has been detected in *Chlorella* species, such as *C. amblystomatis*, *C. sorokiniana*, and *C. vulgaris* (Yun et al. 2020, Conde et al. 2021). The TOF-MS and MS/MS chromatograms in positive ion mode of peak 25 (t_R = 29.0 min) showed an identical molecular ion ($[M+H]^+$) at *m/z* 395.3280 (25A in Supplementary Fig. S2B) and four fragmentation ions (*m/z* 377.3202, –18 amu; *m/z* 251.1794, –144 amu; *m/z* 211.1479, 184 amu; and *m/z* 125.1329, –270 amu) (25B in Supplementary Fig. S2B). The precursor ion at *m/z* 377.3202 resulted from the loss of a dehydrated molecular ion ($[M+H-18, -H_2O]^+$) and the fragment ion at *m/z* 125.1329 was a common pattern formed from the primary cleavage of the C17–C20 bond in the sterol side chain (270 amu). Additionally, the major fragment at *m/z* 211.1479 was formed by the loss of an *m/z* 184 fragment (*m/z* 395.3280 → *m/z* 211.1479: ($[M+H]^+$–{H_2O+(C–D) ring cleavage}) + side chain of sterol) (West and Reid 2021, Feng et al. 2022). The major ion was observed at *m/z* 251.1794, which was formed by the loss of *m/z* 144 fragment (*m/z* 395 → *m/z* 251; {$[M+H]^+$ – (A ring cleavage: C1;4–C5;10) + (C23–C24 cleavage in side chain)}) (Feng et al. 2022). According to the above observations, this peak was assumed to be 9,11-dehydroergosterol ($C_{28}H_{42}O$) (**25**). The TOF-MS and MS/MS profiles of peak 35 (t_R = 39.8 min) displayed a molecular ion $[M+H]^+$ at *m/z* 429.3693, with one main fragment ion at *m/z* 165.0908 (35A and 35B in Supplementary Fig. S2B). The major ion at *m/z* 165.0908 was characteristic of a $C_{10}H_{13}O_2$ moiety, and the lost fragment (–264 amu) corresponded to an alkylchain (16-carbonside chain) residue (Montoya-Arroyo et al. 2022). These findings are in agreement with the earlier result that 11'-α-tocomonoenol was present in cultured microalgae (*C. sorokiniana*, *N. limnetica*, and *T. suecica*) (Montoya-Arroyo et al. 2022). On the basis of the UPLC-TOF-MS analysis, we determined the peak number, elemental formula, retention times, and mass spectral values, including the molecular and fragmentation ions of the total metabolite compositions (Table 1). The present research was undertaken to provide information on a rapid and sensitive method for the identification of 26 (negative) and 36 (positive) metabolites in different ion modes by UPLC-TOF-MS analysis of *C. fusca* (Fig. 3). Moreover, the identified metabolite profiles revealed remarkable differences in the individual and total compositions between the two modes (Fig. 4). These data are useful for evaluating the development of human health agents using *C. fusca*. To the best of our knowledge, the present results document, for the first time, the metabolite compositions as determined by different ion modes using UPLC-TOF-MS/MS.

CONCLUSION

Our work represents the first presentation of detailed information concerning various metabolites through UPLC-TOF-MS in both negative and positive ion modes from a methanol extract of *C. fusca*. A total of 62 components (26 in the negative mode and 36 in the positive mode) were simultaneously identified, and their chemical structures were markedly distinct in the two ion modes, organized as fatty acid > chlorophyll > polar lipid > carotenoid. Moreover, this source exhibited high biological capacities in the rank order of tyrosinase > ABTS > elastase > DPPH; specifically, the ABTS radical was observed to have approximately 3 times higher scavenging activity (90%) than DPPH (34%) at 200 μg mL^{-1}. The enzymatic inhibitions of tyrosinase and elastase also revealed significant differences in ratios greater than 50% (tyrosinase: 93.4 → 61.1% at 140 μg mL^{-1}; elastase: 90.5 → 52.0% at 200 μg mL^{-1}) over 30 min. These findings may be utilized as basic data to maximize the efficiency and industrial applications of *C. fusca*. Our results provide important information for the practical application of *Chlorella* in the development of agricultural and nutraceutical agents. Further studies on high-value metabolites and biofuel production will improve the economics of commercial-scale cultivation of *Chlorella* species.

ACKNOWLEDGEMENTS

This work was carried out with the support of "Cooperative Research Program for Agriculture Science and Technology Development (Project No. PJ015641)" Rural Development Administration, Republic of Korea. Also, this

research was supported by the Basic Science Research Program through the National Research Foundation of Korea (NRF) funded by the Ministry of Education (Grant number 2020R1A6A1A03047729), Republic of Korea, and the Biomaterials Specialized Graduate Program through the Korea Environmental Industry & Technology Institute (KEITI) funded by the Ministry of Environment (MOE).

CONFLICTS OF INTEREST

The authors declare that they have no potential conflicts of interest.

SUPPLEMENTARY MATERIALS

Supplementary Fig. S1. Appearance of *Chlorella fusca* (CHK0059) (https://www.e-algae.org).

Supplementary Fig. S2. Ultra-high performance liquid chromatography coupled with quadrupole time-of-flight mass spectrometry (UPLC-Q-TOF-MS/MS) spectra through mass fragmentation patterns of the identified metabolites (https://www.e-algae.org).

REFERENCES

Ando, H., Watabe, H., Valencia, J. C., et al. 2004. Fatty acid regulate pigmentation via proteasomal degradation of tyrosinase: a new aspect of ubiquitin-proteasome function. J. Biol. Chem. 279:15427–15433. doi.org/10.1074/jbc.M313701200

Azmi, N., Hashim, P., Hashim, D. M., Halimoon, N. & Majid, N. M. N. 2014. Anti-elastase, anti-tyrosinase and matrix metalloproteinase-1 inhibitory activity of earthworm extracts as potential new anti-aging agent. Asian Pac. J. Trop. Biomed. 4(Suppl 1):S348–S352. doi.org/10.12980/APJTB.4.2014C1166

Bock, C., Krienitz, L. & Pröschold, T. 2011. Taxonomic reassessment of the genus *Chlorella* (Trebouxiophyceae) using molecular signatures (barcodes), including description of seven new species. Fottea 11:293–312. doi.org/10.5507/fot.2011.028

Calvano, C. D., Bianco, M., Ventura, G., Losito, I., Palmisano, F. & Cataldi, T. R. I. 2020. Analysis of phospholipids, lysophospholipids, and their linked fatty acyl chains in yellow lupin seeds (*Lupinus luteus* L.) by liquid chromatography and tandem mass spectrometry. Molecules 25:805. doi.org/10.3390/molecules25040805

Canelli, G., Tevere, S., Jaquenod, L., et al. 2022. A novel strategy to simultaneously enhance bioaccessible lipids and antioxidants in hetero/mixotrophic *Chlorella vulgaris* as functional ingredient. Bioresour. Technol. 347:126744. doi.org/10.1016/j.biortech.2022.126744

Chae, H., Kim, E. J., Kim, H. S., Choi, H. G., Kim, S. & Kim, J. H. 2023. Morphology and phylogenetic relationships of two Antarctic strains within the genera *Carolibrandtia* and *Chlorella* (Chlorellaceae, Trebouxiophyceae). Algae 38:241–252. doi.org/10.4490/algae.2023.38.11.30

Chen, K., Ríos, J. J., Pérez-Gálvez, A. & Roca, M. 2015*a*. Development of an accurate and high-through put methodology for structural comprehension of chlorophylls derivatives. (I) Phytylated derivatives. J. Chromatogr. A 1406:99–108. doi.org/10.1016/j.chroma.2015.05.072

Chen, K., Ríos, J. J., Roca, M. & Pérez-Gálvez, A. 2015*b*. Development of an accurate and high-through put methodology for structural comprehension of chlorophylls derivatives. (II) Dephytylated derivatives. J. Chromatogr. A 1412:90–99. doi.org/10.1016/j.chroma.2015.08.007

Cholewski, M., Tomczykowa, M. & Tomczyk, M. 2018. A comprehensive review of chemistry, sources and bioavailability of omega-3 fatty acids. Nutrients 10:1662. doi.org/10.3390/nu10111662

Conde, T. A., Couto, D., Melo, T., et al. 2021. Polar lipidomic profile shows *Chlorococcum amblystomatis* as a promising source of value-added lipids. Sci. Rep. 11:4355. doi.org/10.1038/s41598-021-83455-y

Deamici, K. M., Santos, L. O. & Costa, J. A. V. 2019. Use of static magnetic fields to increase CO_2 biofixation by the microalga *Chlorella fusca*. Bioresour. Technol. 276:103–109. doi.org/10.1016/j.biortech.2018.12.080

EI-fayoumy, E. A., Shanab, S. M. M., Gaballa, H. S., Tantawy, M. A. & Shalaby, E. A. 2021. Evaluation of antioxidant and anticancer activity of crude extract and different fractions of *Chlorella vulgaris* axenic culture grown under various concentrations of copper ions. BMC Complement. Med. Ther. 21:51. doi.org/10.1186/s12906-020-03194-x

Feng, M., Jin, Y., Yang, S., et al. 2022. Sterol profiling of *Leishmania* parasites using a new HPLC-tandem mass spectrometry-based method and antifungal azoles as chemical probes reveals a key intermediate sterol that supports a branched ergosterol biosynthetic pathway. Int. J. Parasitol. Drugs Drug Resist. 20:27–42. doi.org/10.1016/j.ijpddr.2022.07.003

Ferdous, U. T., Nurdin, A., Ismail, S. & Yusof, Z. N. B. 2023. Evaluation of the antioxidant and cytotoxic activities of crude extracts from marine *Chlorella* sp. Biocatal. Agric. Biotechnol. 47:102551. doi.org/10.1016/j.

bcab.2022.102551

Fernandes, T. & Cordeiro, N. 2020. *Hemiselmis andersenii* and *Chlorella stigmatophora* as new sources of high-value compounds: a lipidomic approach. J. Phycol. 56:1493–1504. doi.org/10.1111/jpy.13042

Gorgich, M., Martins, A. A., Mata, T. M. & Caetano, N. S. 2021. Composition, cultivation and potential applications *Chlorella zofingiensis*: a comprehensive review. Algal Res. 60:102508. doi.org/10.1016/j.algal.2021.102508

Ha, T. J., Park, J. E., Lee, K.-S., et al. 2021. Identification of anthocyanin compositions in black seed coated Korean adzuki bean (*Vigna angularis*) by NMR and UPLC-Q-Orbitrap-MS/MS and screening for their antioxidant properties using different solvent systems. Food Chem. 346:128882. doi.org/10.1016/j.foodchem.2020.128882

Habashy, N. H., Abu Serie, M. M., Attia, W. E. & Addelgaleil, S. A. M. 2018. Chemical characterization, antioxidant and anti-inflammatory properties of Greek *Thymus vulgaris* extracts and their possible synergism with Egyptian *Chlorella vulgaris*. J. Funct. Foods 40:317–328. doi.org/10.1016/j.jff.2017.11.022

Kang, N., Heo, S.-Y., Kim, E.-A., Ryu, B. & Heo, S.-J. 2023. Antiviral effect of fucoxanthin obtained from *Sargassum siliquastrum* (Fucales, Phaeophyceae) against severe acute respiratory syndrome coronavirus 2. Algae 38:295–306. doi.org/10.4490/algae.2023.38.11.29

Kim, M., Oh, H. J., Nguyen, K. & Jin, E. 2022. Identification and characterization of *Dunaliella salina* OH214 strain newly isolated from a saltpan in Korea. Algae 37:317–329. doi.org/10.4490/algae.2022.37.9.13

Koch, E., Wiebel, M., Hopmann, C., Kampschulte, N. & Schebb, N. H. 2021. Rapid quantification of fatty acids in plant oils and biological samples by LC-MS. Anal. Bioanal. Chem. 413:5439–5451. doi.org/10.1007/s00216-021-03525-y

Kotrbáček, V., Doubek, J. & Doucha, J. 2015. The chlorococcalean alga *Chlorella* in animal nutrition: a review. J. Appl. Phycol. 27:2173–2180. doi.org/10.1007/s10811-014-0516-y

Lee, J. H., Seo, E. Y. & Lee, Y. M. 2023. Comparative investigation on variations of nutritional components in whole seeds and seed coats of Korean black soybeans for different crop years and screening of their antioxidant and anti-aging properties. Food Chem. X 17:100572. doi.org/10.1016/j.fochx.2023.100572

Li, C., Wurst, K., Berghold, J., Podewitz, M., Liedl, K. R. & Kräutler, B. 2018. Pyro-phyllobilins: elusive chlorophyll catabolites lacking a critical carboxylate function of the natural chlorophylls. Chem. Eur. J. 24:2987–2998. doi.org/10.1002/chem.201705331

López-Pacheco, I. Y., Salinas-Salazar, C., Silva-Núñez, A., et al. 2019. Removal and biotransformation of 4-nonylphenol by *Arthrospira maxima* and *Chlorella vulgaris* consortium. Environ. Res. 179:108848. doi.org/10.1016/j.envres.2019.108848

Martini, F., Beghini, G., Zanin, L., Varanini, Z., Zamboni, A. & Ballottari, M. 2021. The potential use of *Chlamydomonas reinhardtii* and *Chlorella sorokiniana* as biostimulants on maize plants. Algal Res. 60:102515. doi.org/10.1016/j.algal.2021.102515

Mata, T. M., Martins, A. A. & Caetano, N. S. 2010. Microalgae for biodiesel production and other applications: a review. Renew. Sust. Energ. Rev. 14:217–232. doi.org/10.1016/j.rser.2009.07.020

Molnár, P., Deli, J., Ősz, E., et al. 2006. Preparation and spectroscopic characterization of 3'-oxolutein. Lett. Org. Chem. 3:723–734. doi.org/10.2174/157017806779025933

Montes D'Oca, M. G., Viêgas, C. V., Lemões, J. S., et al. 2011. Production of FAMEs from several microalgal lipidic extracts and direct transesterification of the *Chlorella pyrenoidosa*. Biomass Bioenerg. 35:1533–1538. doi.org/10.1016/j.biombioe.2010.12.047

Montoya-Arroyo, A., Lehnert, K., Muñoz-González, A., Schmid-Staiger, U., Velter, W. & Frank, J. 2022. Tocochromanol profiles in *Chlorella sorokiniana*, *Nannochloropsis limnetica*, and *Tetraselmis suecica* confirm the presence of 11'-α-tocomonoenol in cultured microalgae independently of species and origin. Foods 11:396. doi.org/10.3390/foods11030396

Moser, S., Erhart, T., Neuhauser, S. & Kräutler, B. 2020. Phyllobilins from senescence-associated chlorophyll breakdown in the leaves of Basil (*Ocimum basilicum*) show increased abundance upon herbivore attack. J. Agric. Food Chem. 68:7132–7142. doi.org/10.1021/acs.jafc.0c02238

Musharraf, S. G., Ahmed, M. A., Zehra, N., Kabir, N., Choudhary, M. I. & Rahman, A.-U. 2012. Biodiesel production from microalgal isolates of southern Pakistan and quantification of FAMEs by GC-MS/MS analysis. Chem. Cent. J. 6:149. doi.org/10.1186/1752-153X-6-149

Nilsson, T., Martínez, E., Manresa, A. & Oliw, E. H. 2010. Liquid chromatography/tandem mass spectrometric analysis of 7,10-dihydroxyoctadecenoic acid, its isotopomers, and other 7,10-dihydroxy fatty acids formed by *Pseudomonas aeruginosa* 42A2. Rapid Commun. Mass Spectrom. 24:777–783. doi.org/10.1002/rcm.4446

Pantami, H. A., Bustamam, M. S. A., Lee, S. Y., et al. 2020. Comprehensive GC-MS and LC-MS/MS metabolite profiling of *Chlorella vulgaris*. Mar. Drugs 18:367. doi.org/10.3390/md18070367

Rahman, M. J., Ambigaipalan, P. & Shahidi, F. 2018. Biological activities of Camelina and Sophia seeds phenolics: inhibition of LDL oxidation, DNA damage, and pancreatic lipase and α-glucosidase activities. J. Food Sci. 83:237–245. doi.org/10.1111/1750-3841.14007

Rivera, S. M., Christou, P. & Canela-Garayoa, R. 2014. Identification of carotenoids using mass spectrometry. Mass Spectrom. Rev. 33:353–372. doi.org/10.1002/mas.21390

Safarfar, H., van Wagenen, J., Møller, P. & Jacobsen, C. 2015. Carotenoids, phenolic compounds and tocopherols contribute to the antioxidative properties of some microalgae species grown on industrial wastewater. Mar. Drugs 13:7339–7356. doi.org/10.3390/md13127069

Safi, C., Zebib, B., Merah, O., Pontalier, P.-Y. & Vaca-Garcia, C. 2014. Morphology, composition, production, processing and applications of *Chlorella vulgaris*: a review. Renew. Sustain. Energy Rev. 35:265–278. doi.org/10.1016/j.rser.2014.04.007

Seal, T., Chaudhuri, K., Pillai, B., Chakrabarti, S., Mondal, T. & Auddy, B. 2020. Evaluation of antioxidant activities, toxicity studies and the DNA damage protective effect of various solvent extracts of *Litsea cubeba* fruits. Heliyon 6:e03637. doi.org/10.1016/j.heliyon.2020.e03637

Shimma, S., Kubo, A., Satoh, T. & Toyoda, M. 2012. Detailed structural analysis of lipids directly on tissue specimens using a MALDI-spiralTOF-reflectron TOF mass spectrometer. PLoS ONE 7:e37107. doi.org/10.1371/journal.pone.0037107

Sotoudehniakarani, F., Alayat, A. & McDonald, A. G. 2019. Characterization and comparison of pyrolysis products from fast pyrolysis of commercial *Chlorella vulgaris* and cultivated microalgae. J. Anal. Appl. Pyrolysis 139:258–273. doi.org/10.1016/j.jaap.2019.02.014

Stigter, E. C. A., Letsiou, S., vd Broek, N. J. F., et al. 2013. Development and validation of a quantitative LC-tandem MS assay for hexadeca-4,7,10,13-tetraenoic acid in human and mouse plasma. J. Chromatogr. B 925:16–19. doi.org/10.1016/j.jchromb.2013.01.012

Vello, V., Umashankar, S., Phang, S.-M., et al. 2018. Metabolomic profiles of tropical *Chlorella* and *Parachlorella* species in response to physiological changes during exponential and stationary growth phase. Algal Res. 35:61–75. doi.org/10.1016/j.algal.2018.08.014

Viera, I., Roca, M. & Pérez-Gálvez, A. 2018. Mass spectrometry of non-allomerized chlorophylls a and b derivatives from plants. Curr. Org. Chem. 22:842–876. doi.org/10.2174/1385272821666170920164836

West, H. & Reid, G. E. 2021. Hybrid 213 nm photodissociation of cationized sterol lipid ions yield $[M]^+$: radical products for improved structural characterization using multistage tandem mass spectrometry. Anal. Clim. Acta 1141:100–109. doi.org/10.1016/j.aca.2020.10.013

Won, H., Ro, E., Seo, S., Kim, B.-H. & Jin, E. S. 2023. Isolation and cultivation of freshwater diatom *Nitzschia palea* HY1 for increasing biomass and fucoxanthin production. Algae 38:191–202. doi.org/10.4490/algae.2023.38.9.3

Yun, H.-S., Kim, Y.-S. & Yoon, H.-S. 2020. Characterization of *Chlorella sorokiniana* and *Chlorella vulgaris* fatty acid components under a wide range of light intensity and growth temperature for their use as biological resources. Heliyon 6:e04447. doi.org/10.1016/j.heliyon.2020.e04447

Zhou, J., Wang, M., Bäuerl, C., et al. 2023. The impact of liquid-pressurized extracts of *Spirulina*, *Chlorella* and *Phaedactylum tricornutum* on *in vitro* antioxidant, antiinflammatory and bacterial growth effects and gut microbiota modulation. Food Chem. 401:134083. doi.org/10.1016/j.foodchem.2022.134083

Zhou, J., Wang, M., Saraiva, J. A., et al. 2022. Extraction of lipids from microalgae using classical and innovative approaches. Food Chem. 384:132236. doi.org/10.1016/j.foodchem.2022.132236